Cell Host & Microbe
Article

KSHV-Initiated Notch Activation Leads to Membrane-Type-1 Matrix Metalloproteinase-Dependent Lymphatic Endothelial-to-Mesenchymal Transition

Fang Cheng,[1,2,9] Pirita Pekkonen,[1,2,9] Simonas Laurinavicius,[2,8,9] Nami Sugiyama,[2] Stephen Henderson,[4] Thomas Günther,[5] Ville Rantanen,[2] Elisa Kaivanto,[1,2] Mervi Aavikko,[2] Grzegorz Sarek,[1,2] Sampsa Hautaniemi,[2] Peter Biberfeld,[6] Lauri Aaltonen,[2] Adam Grundhoff,[5] Chris Boshoff,[4] Kari Alitalo,[3] Kaisa Lehti,[2,10] and Päivi M. Ojala[1,2,7,10,*]
[1]Institute of Biotechnology, University of Helsinki, P.O. Box 56, 00014 Helsinki, Finland
[2]Research Programs Unit, Genome-Scale Biology, Biomedicum Helsinki and Institute of Biomedicine
[3]Research Programs Unit, Molecular Cancer Biology, Biomedicum Helsinki and Haartman Institute
University of Helsinki, P.O. Box 63, 00014 Helsinki, Finland
[4]Cancer Research UK, University College London Cancer Institute, University College London, London WC1E 6BT, UK
[5]Heinrich Pette Institute - Leibniz Institute for Experimental Virology, Martinistrasse 52, 20251 Hamburg, Germany
[6]Department of Pathology and Oncology, Karolinska Institute, Stockholm SE-171 77, Sweden
[7]Foundation for the Finnish Cancer Institute
[8]Present address: Department of Immunology and Cell Biology, Institute of Biotechnology, Vilnius University, Graiciuno 8, 02241 Vilnius, Lithuania
[9]These authors contributed equally to this work
[10]These authors contributed equally to this work
*Correspondence: paivi.ojala@helsinki.fi
DOI 10.1016/j.chom.2011.10.011

SUMMARY

Kaposi sarcoma (KS), an angioproliferative disease associated with Kaposi sarcoma herpesvirus (KSHV) infection, harbors a diversity of cell types ranging from endothelial to mesenchymal cells of unclear origin. We developed a three-dimensional cell model for KSHV infection and used it to demonstrate that KSHV induces transcriptional reprogramming of lymphatic endothelial cells to mesenchymal cells via endothelial-to-mesenchymal transition (EndMT). KSHV-induced EndMT was initiated by the viral proteins vFLIP and vGPCR through Notch pathway activation, leading to gain of membrane-type-1 matrix metalloproteinase (MT1-MMP)-dependent invasive properties and concomitant changes in viral gene expression. Mesenchymal markers and MT1-MMP were found codistributed with a KSHV marker in the same cells from primary KS biopsies. Our data explain the heterogeneity of cell types within KS lesions and suggest that KSHV-induced EndMT may contribute to KS development by giving rise to infected, invasive cells while providing the virus a permissive cellular microenvironment for efficient spread.

INTRODUCTION

Kaposi's sarcoma herpesvirus (KSHV) is the etiological agent for Kaposi's sarcoma (KS), an angioproliferative disease characterized by a prominent compartment of spindle cells that are considered to be the tumor cells of KS (Ganem, 2010). Despite extensive studies, the origin of the cells characterizing the KS lesion is not established as the tumors are composed of quite heterogenic populations of cells expressing markers of endothelial cells (ECs) (Dupin et al., 1999; Kaaya et al., 1995), smooth muscle cells, and fibroblasts (Kaaya et al., 1995; Stürzl et al., 1995; Weich et al., 1991). The prevailing view is that KS is derived from endothelial cells (Ganem, 2010). KSHV infects various types of ECs in culture, and they represent a useful model system for studies on KSHV pathogenesis (McAllister and Moses, 2007).

Despite the apparent susceptibility of ECs, and especially lymphatic ECs (LECs) to KSHV infection, primary ECs infected with wild-type KSHV do not readily acquire properties of transformed cells, and tend to lose the viral episomes upon culturing (Grundhoff and Ganem, 2004). We and others have shown that KSHV infection evokes antiproliferative, rather than proliferative, responses in cultured ECs (Koopal et al., 2007; Lagunoff et al., 2002), making aspects of KS tumorigenesis difficult to study in vitro. Interestingly, growth suppression induced by recombinant KSHV in endothelial precursor cells could be overcome by implantation of the cells into mice, which resulted in the development of KS-like tumors (Mutlu et al., 2007). This suggests that the tumorigenic potential of KSHV is dependent on the tissue microenvironment. Since crosslinked three-dimensional (3D) matrices can mimic certain important aspects of the tissue environment (Rowe and Weiss, 2009), we sought to identify cellular pathways and virus-host interactions involved in KSHV pathogenesis by using a 3D, organotypic model for KSHV-infected primary LECs.

RESULTS

Mesenchymal Cells in KS Lesions Are Infected with KSHV

Spindle cells with heterogeneous mesenchymal marker expression of unclear origin have been reported in KS lesions

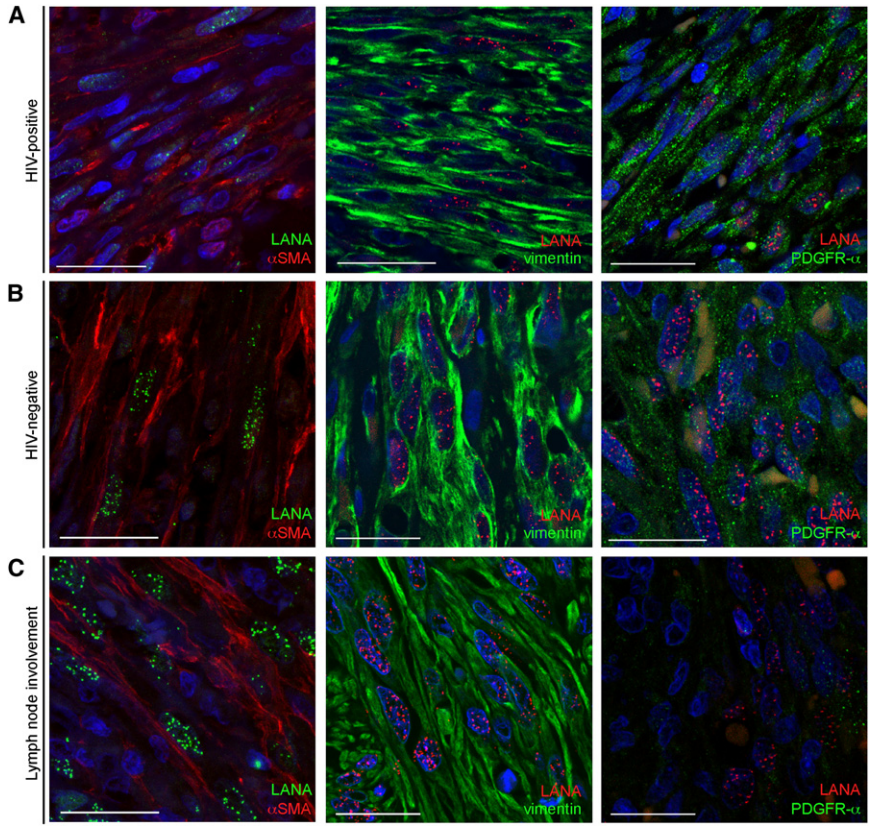

Figure 1. Mesenchymal Cells in Primary KS Tumors Are Infected with KSHV

Codistribution of LANA (punctate green signal) and αSMA (red; left panels), LANA (punctate red signal) and vimentin (green; middle panels), and LANA (punctate red signal) and PDGFR-α (green; right panels) in the same cells in sections of nodular KS biopsies from HIV-positive (A) and HIV-negative (B) patients, as well as in a KS lymph node involvement from an HIV-negative patient (C). Nuclei were counterstained with Hoechst 33342 (blue). Scale bars represent 25 μm. See also Figure S1 and Table S1.

(Kaaya et al., 1995; Stürzl et al., 1995; Weich et al., 1991). To define the KSHV-infection status of these mesenchymal cells, we double-labeled human KS biopsies for the KSHV latency associated nuclear antigen (LANA) and mesenchymal markers (α-smooth muscle actin [αSMA], vimentin, and PDGFR-α). The KSHV-infected cells were distinguished by the typical punctate staining of LANA in the cell nucleus. Cells coexpressing αSMA and LANA were found in 10 out of 14 of the primary tumors from HIV-positive or HIV-negative patients and in a lymph node involvement of KS (Figure 1 and Figure S1 available online). Based on a quantitative image analysis the overall percentage of cells showing codistribution of LANA and αSMA was relatively low (Table S1). Interestingly, most of these cells localized close to the interface of the tumor and the stroma (Figures S1E and S1F). Cells double positive for LANA and fibrous vimentin were detected in all of the KS biopsies (14/14) and in the single lymph node involvement analyzed (Figure 1 and Figure S1). Furthermore, seven out of eight tumors contained cells positive for both PDGFR-α and LANA (Figures 1A and 1B and Figure S1A, S1B, S1D, and S1E). Whereas vimentin was observed also in LANA-negative, noninfected cells, the LANA-positive cells displayed a stronger, fibrous vimentin signal (Table S1 and Figure S1G). The uninfected, vimentin-expressing cells within tumors may represent activated stromal fibroblasts or infiltrating lymphocytes. These findings indicate that a substantial amount of the cells with mesenchymal marker expression in KS lesions are KSHV positive.

KSHV Induces Endothelial-to-Mesenchymal Transition in LEC Spheroids

KSHV induces reprogramming of blood ECs (BECs) to LECs (and vice versa) in two-dimensional (2D) cultures. Furthermore, the KS gene expression signature resembles more that of LECs than BECs (Carroll et al., 2004; Hong et al., 2004; Wang et al., 2004). To investigate whether KSHV infection could induce reprogramming of ECs to the mesenchymal cells that we observed in the KS lesions, we infected differentiated, primary LECs with KSHV, and established a 3D cell model to provide a more physiological environment for the cells. The 3D organotypic culture is based on the property of ECs to form spheroids under nonadherent conditions (Korff and Augustin, 1998), and it has proven useful for studies on endothelial capillary sprouting. Spheroids were prepared from KSHV-infected LECs (K-LECs) and uninfected control LECs seven to ten days after infection and monitored for 5 days. KSHV induced a dramatic outgrowth of fibroblast-like cells in the LEC spheroids whereas minimal sprouting was observed in control LECs (Figure 2A and Figure S2A). Although a little outgrowth of sprouts was occasionally observed in the control LEC spheroids, these were tube-like structures with the expression of PECAM-1 in the cell-cell junctions typical for endothelial capillaries (Figure S2B).

Expression of mesenchymal proteins (αSMA, transgelin, N-cadherin, fibronectin, and fibrous vimentin) was strongly induced in the sprouts (but less so in the body) of the K-LEC spheroids, but not in LEC control spheroids (Figure 2B). The upregulation of *TAGLN*, *VIM*, and *CDH2*, as well as a panel of other mesenchymal markers (*CNN1*, *PDGFRB*, *COL1A1*, and *S100A4*) was confirmed by quantitative reverse-transcriptase PCR (qRT-PCR; Figure 2C). Importantly, none of these markers were induced in the parental 2D K-LECs (Figure 2C), suggesting that the 3D environment triggered the transition of K-LECs into a mesenchymal phenotype.

To determine whether induction of mesenchymal markers in the K-LEC spheroids was associated with changes in the EC state, we detected EC markers in the spheroids. In accordance with previous reports showing KSHV-induced downregulation of EC markers in 2D (Mansouri et al., 2006; Qian et al.,

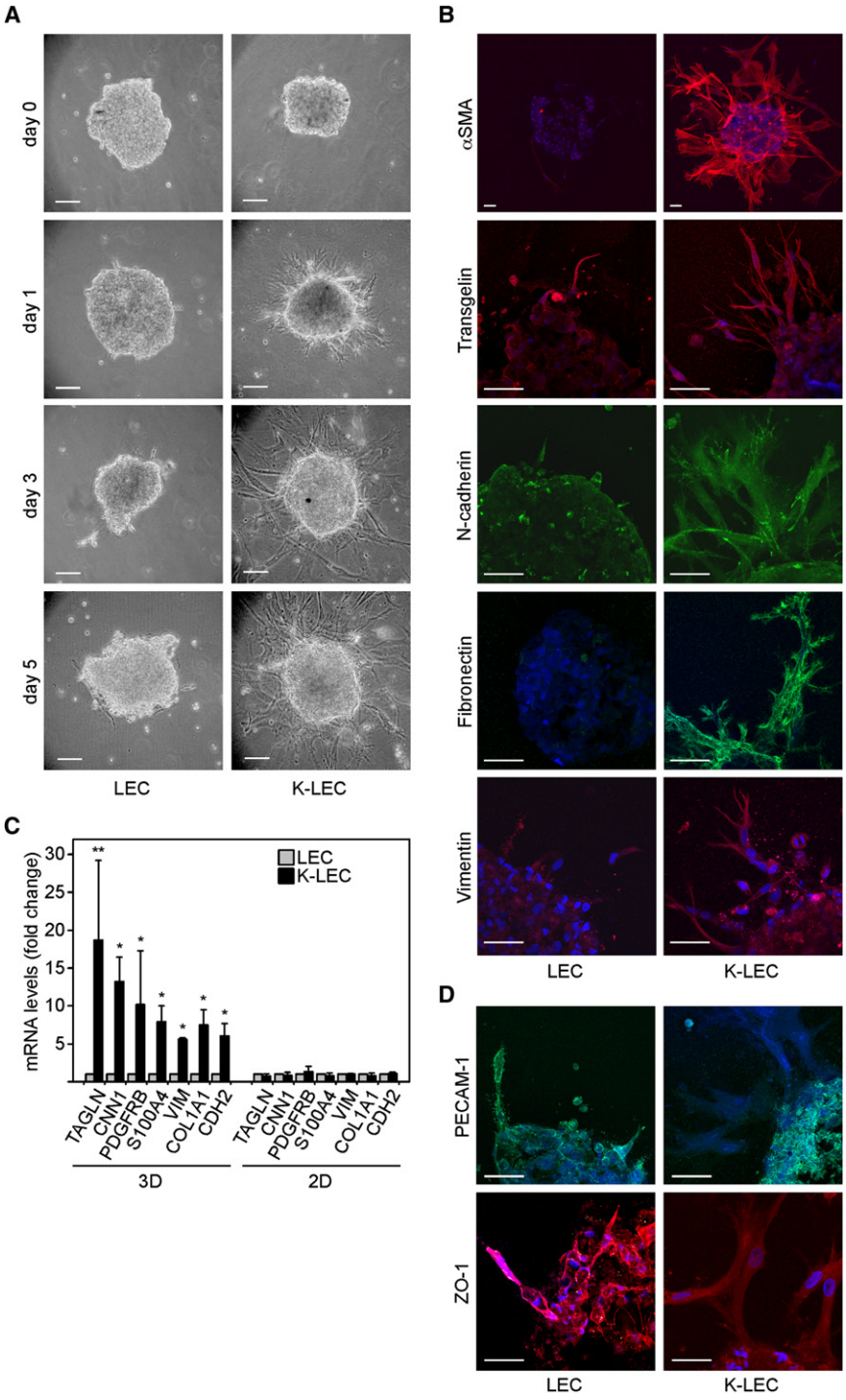

Figure 2. KSHV Induces Primary LECs to Undergo EndMT in 3D

(A) Sprouting time course of LEC and K-LEC spheroids after embedding into 3D.

(B) Expression of αSMA, transgelin, vimentin (in red), N-cadherin, and fibronectin (in green) in LEC and K-LEC spheroids.

(C) qRT-PCR analysis of transcripts for the indicated mesenchymal genes in LEC and K-LEC spheroids (3D) and their parental 2D cultures. Error bars represent mean fold change with respect to LEC ± SD; n = 2–4.

(D) Expression of PECAM-1 (in green) and ZO-1 (in red) in LEC and K-LEC spheroids.

The nuclei in (B) and (D) were counterstained with Hoechst 33342 (blue). Scale bars in (A), (B), and (D) represent 50 μm. See also Figure S2.

2008), EC marker (VE-cadherin) and LEC markers (VEGFR3 and LYVE1) were downregulated in the 2D K-LECs (Figure S2C). Futhermore, PECAM-1, a ubiquitous EC protein and two LEC markers (VEGFR3 and podoplanin) were notably downregulated in the mesenchymal marker expressing K-LEC sprouts (Figure 2D and Figure S2D) with a simultaneous induction of fibronectin in the sprouts and at the outer rim of the spheroid body of the K-LECs (Figure S2D). LEC marker downregulation was further confirmed by qRT-PCR for *PROX1* and *FLT4* (VEGFR3) genes both in 2D and 3D K-LECs (Figure S2E).

These data strongly suggest that in the 3D environment KSHV infection not only suppresses expression of LEC markers, but can also induce LECs to differentiate into a new, mesenchymal cell type via endothelial-to-mesenchymal transition (EndMT) (Potenta et al., 2008). This process of cellular plasticity is analogous to epithelial-to-mesenchymal transition (EMT) with a recently proposed role in tumor progression and metastasis and as a source for cancer-associated fibroblasts and multipotent stem cells (Kalluri and Weinberg, 2009). As a further confirmation of EndMT and loss of polarity, we observed a clear relocalization of the tight-junction protein ZO-1 from the cell-cell contacts in control LEC spheroids to more disperse, cytoplasmic localization in the sprouts of K-LEC spheroids (Figure 2D).

KSHV-Infection Is Required for Extensive Sprouting of LECs in 3D

To test whether the K-LEC sprouting required infectious virus, we formed spheroids of LECs infected with UV-inactivated virus (UV-K-LEC). Whereas the control K-LEC spheroids sprouted efficiently, minimal sprouting was observed in the UV-K-LEC spheroids (Figures 3A and 3B). This suggests that infectious KSHV rather than viral surface proteins or factors originating from the virus preparation is required for sprout outgrowth. To define the contribution of infected cells in sprout formation, spheroids were prepared from a 1:3 mixture of GFP-expressing rKSHV.219-infected LECs and control LECs. GFP was observed in most of the sprouts suggesting that infected cells were

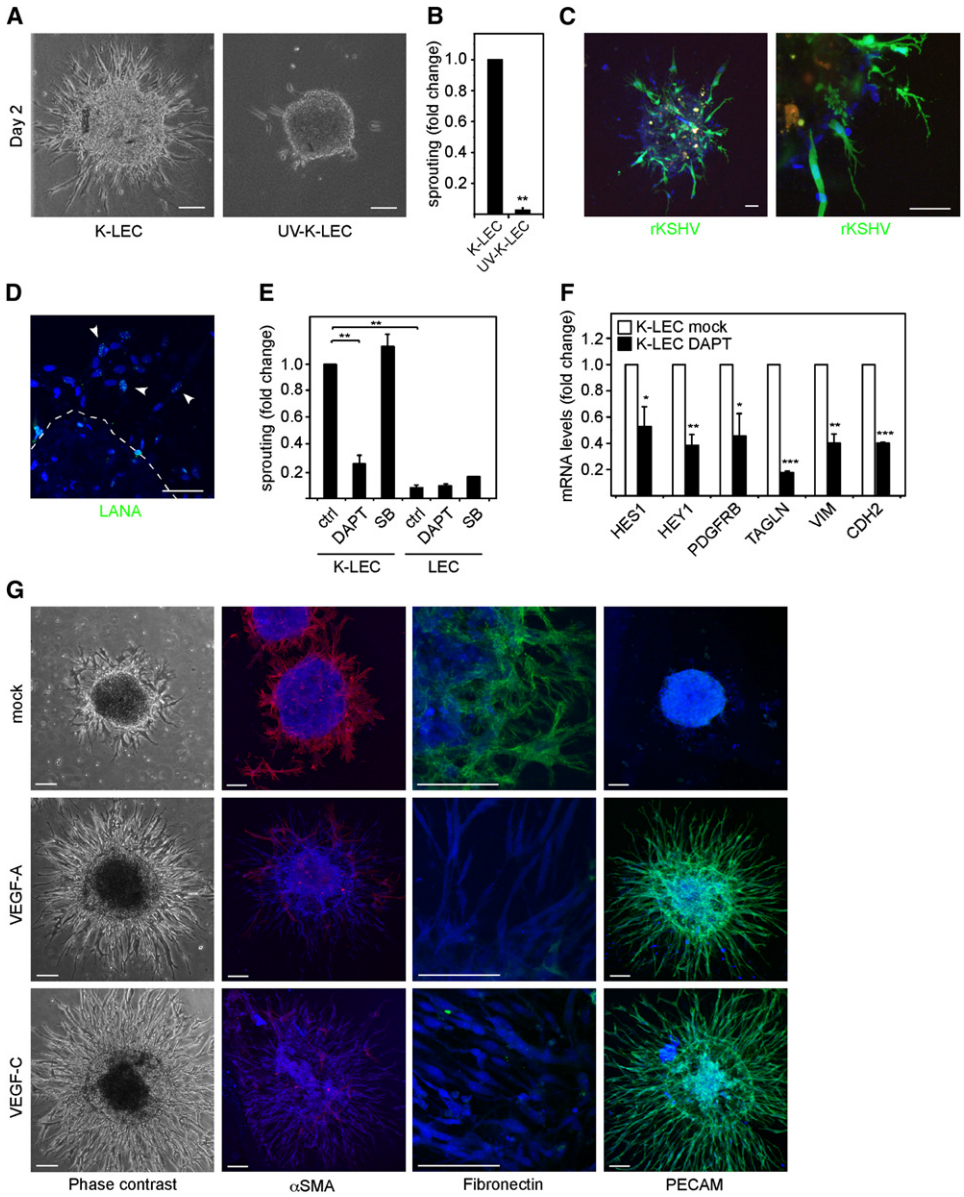

Figure 3. KSHV-Induced EndMT Requires Infectious Virus and Is Positively Regulated by Notch but Inhibited by VEGF Stimulation

(A) Phase-contrast images of spheroids prepared from K-LECs and LECs infected with UV-inactivated KSHV (UV-K-LEC).

(B) Loss of sprouting in UV-K-LEC spheroids normalized to K-LEC.

(C) Confocal images of uninfected and GFP-expressing rK-LECs mixed in a 3:1 ratio to form spheroids.

(D) Confocal image of K-LEC spheroid stained with anti-LANA antibodies (green punctate nuclear signal). Dashed line denotes the spheroid body area and arrowheads point examples of LANA-positive cells in the sprouts.

(E) Sprouting of LEC and K-LEC spheroids treated with DAPT or SB431542 (SB) compared to the corresponding vehicle K-LEC controls (ctrl).

(F) qRT-PCR analysis for the Notch downstream target genes *HES1*, *HEY1* and the indicated mesenchymal markers in K-LEC spheroids in relation to vehicle K-LEC control (mock).

(G) Sprouting and expression of mesenchymal markers (αSMA in red, and fibronectin in green) and the endothelial marker (PECAM in green) of the spheroids prepared from mock-, VEGF-A-, or VEGF-C-stimulated K-LECs.

± SEM is shown; n = 2 (B, E, [SB], and F) and n = 3 (E [DAPT]). *p < 0.05, **p < 0.01, ***p < 0.001 (B, D, and F). Nuclei in (C), (D), and (G) were counterstained with Hoechst 33342 (blue). Scale bars represent 100 μm (A and G) and 50 μm (C and D). See also Figure S3.

predominantly contributing to the sprouting (Figure 3C). In addition, majority of the sprouting cells in 3D KLEC cultures expressed KSHV LANA in majority of the sprouting cells (Figure 3D).

Notch Pathway Activation Initiates the KSHV-Induced EndMT

EndMT induction has been described in response to activation of the TGF-β or Notch pathways (Medici et al., 2010; Noseda et al.,

2004; Timmerman et al., 2004). To elucidate the signaling pathways involved in the KSHV-induced EndMT, the spheroids were treated with the inhibitor of TGF-β downstream kinases ALK4, ALK5, ALK7 (SB431542), or an inhibiting antibody for TGF-β (anti-TGF-β) upon embedding in fibrin, while the Notch pathway was inhibited using a gamma-secretase inhibitor (DAPT) or a soluble inhibitor of Dll4/Notch signaling (Dll4-Fc). SB431542 (Figure 3E) or anti-TGF-β (data not shown) did not inhibit sprouting of the K-LEC spheroids or affect the phenotype of control LEC spheroids. KSHV infection alone did not significantly induce any of the tested TGF-β targets (*PAI-1*, *CTGF*, *SNAI1*, and *ZEB1*) in LECs. Although K-LECs were responsive to TGF-β stimulation (Figure S3B) it did not significantly affect sprouting or the expression of Notch and the mesenchymal transcripts in the K-LEC spheroids (Figures S3A and S3B). Induction of all the TGF-β target genes were effectively inhibited by SB431542 in the TGF-β stimulated samples whereas expression of *HES1* and mesenchymal transcripts remained essentially unchanged (Figure S3C).

In contrast, inhibition of the Notch pathway by DAPT or Dll4-Fc dramatically reduced the number of sprouts in the K-LEC spheroids (~4- and 7.5-fold, respectively; Figure 3E and Figure S3D), whereas control LEC spheroids were unaffected. Transcripts for mesenchymal markers such as *TAGLN* (~5.6-fold), *PDGFRB* (~2.5-fold), *VIM* (~2.4-fold), and *CDH2* (~2.5-fold) were decreased accordingly in the DAPT-treated (Figure 3F) and Dll4-Fc-treated K-LEC spheroids (Figure S3E). The involvement of Notch is in line with recent reports demonstrating engagement of Notch signaling in LECs by KSHV (Emuss et al., 2009; Liu et al., 2010). Consistently, the downstream targets of the activated Notch, *HEY1* and *HES1* were induced in K-LECs cultured in both 2D and 3D (data not shown). Taken together, our data suggest that Notch signaling is a major positive regulator of the KSHV-induced EndMT in 3D.

KSHV-Induced EndMT and VEGF-Stimulated Lymphangiogenesis Represent Distinct Biological Processes

Notch signaling has previously been shown to antagonize vascular endothelial growth factor (VEGF) function and to inhibit angiogenic sprouting of HUVECs (BECs) (Ridgway et al., 2006) and lymphangiogenic sprouting of LECs (Zheng et al., 2011) in assays similar to our system. Thus, we compared sprouting of mock-treated K-LEC spheroids to K-LEC spheroids stimulated by VEGF-A or VEGF-C. Light-microscopic analysis revealed outgrowth of the typical mesenchymal-like sprouts from the mock spheroids, whereas both of the VEGF-A or -C stimulated spheroids showed extensive sprouting with apparent capillary morphology (Figure 3G). Confocal microscopy and qRT-PCR analysis further demonstrated that in contrast to the mock, the sprouts in the VEGF-A/C-stimulated spheroids did not express mesenchymal markers (αSMA, fibronectin) but had a strong signal for the EC marker PECAM (Figure 3G and data not shown). These results indicate that the KSHV-induced mesenchymal reprogramming of LECs in 3D is a unique process induced and regulated by different biological stimuli than the (lymph)angiogenic sprouting by VEGF-A/C.

vGPCR and vFLIP Are Involved in the Reprogramming of LECs

Two KSHV encoded proteins were recently shown to engage Notch signaling; the viral FLICE inhibitory protein (vFLIP) through induction of JAG1 and the viral G protein-coupled receptor (vGPCR) through upregulation of DLL4 (Emuss et al., 2009). To investigate whether these viral genes were involved in the KSHV-induced EndMT, LECs were transduced with lentiviruses expressing vGPCR, vFLIP, and an empty control virus (pSIN). As revealed by phase contrast and IF confocal microscopy, vGPCR- and vFLIP-expression in the spheroids induced αSMA and vimentin expressing sprouts (Figure 4A). Accordingly, upregulation of *HES1*, *HEY1*, and mesenchymal markers *TAGLN*, *VIM*, and *CDH2* was seen by qRT-PCR in the vGPCR- and vFLIP-spheroids over the pSIN-spheroids (Figure 4B). Inhibition of Notch by DAPT reduced sprouting of the vGPCR-expressing spheroids by 2-fold (Figure 4C) and induction of the indicated mesenchymal transcripts by 2.1- to 2.7-fold (Figure 4D). DAPT treatment of the vFLIP-expressing spheroids resulted in a milder, but significant decrease both in sprouting (1.3-fold; Figure 4C) and induction of most of the mesenchymal markers (1.4- to 2.0-fold; Figure 4D). This suggests that vFLIP and vGPCR are involved in the activation of KSHV-induced EndMT via Notch. In contrast, lenti- or retroviral expression of the latent genes LANA or v-cyclin, respectively, did not induce sprouting (Figure 4E) or expression of the Notch targets (*SNAI2* and *NRARP*) and mesenchymal markers in the primary LECs (Figure S4A), although LANA has also been implicated in Notch activation (Liu et al., 2010).

To assess the requirement of vFLIP and vGPCR in EndMT in the context of the whole virus infection, we silenced the expression of vFLIP and vGPCR individually or simultaneously in K-LECs. Sprouting of the K-LEC spheroids was reduced for 42% by depletion of vGPCR, for about 36% by vFLIP depletion and for 57% by simultaneous silencing of them both (Figure 4F), which was coupled with the reduction of αSMA and fibronectin expression in the corresponding K-LEC spheroids (Figure 4G). These results indicate that vGPCR and vFLIP coregulate the EndMT in K-LECs.

Cytoskeletal Dynamics Is Essential for the Virus-Induced EndMT in 3D

To test whether sprouting is a prerequisite for the EndMT in the 3D microenvironment, we treated K-LEC spheroids with chemicals disrupting either microtubules (nocodazole) or actin filaments (cytochalasin D). Nocodazole disrupted the fibroblast-like morphology of the sprouts in K-LEC spheroids (Figure S4B) and abolished induction of mesenchymal gene expression, whereas the downstream targets of Notch signaling were unaffected or slightly increased (Figure S4C). As cytochalasin D treatment led to a significant decrease in both Notch signaling and mesenchymal marker expression (data not shown), we were unable to differentiate its specific effect on EndMT. These data suggest that a functional microtubule network (cooperating with the Notch pathway) is essential for the KSHV-induced EndMT.

KSHV-Induced EndMT Endows Primary LECs with Invasive Properties

To obtain a more comprehensive picture of the properties of 3D reprogrammed K-LECs, we compared the gene expression

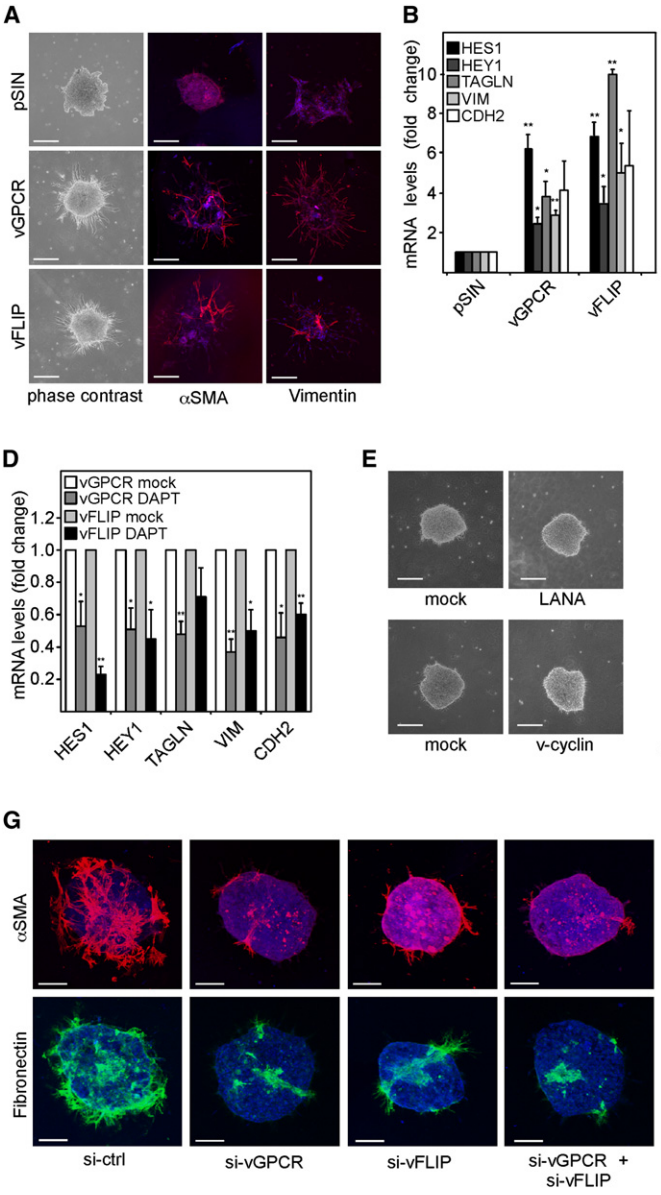

Figure 4. Notch Engagement by vGPCR and vFLIP Is Involved in the KSHV-Induced EndMT

(A) Expression of αSMA (middle panels, in red) and vimentin (right panels, in red) proteins in pSIN-, vGPCR-, and vFLIP-transduced LEC spheroids. Phase contrast images are shown on the left.

(B) Expression of *HES1*, *HEY1* and the indicated mesenchymal transcripts in the spheroids described in (A).

(C) Sprouting of vGPCR- and vFLIP-transduced LEC spheroids treated with DAPT (+) over the vehicle control (–).

(D) Expression of *HES1*, *HEY1* and indicated mesenchymal genes in the vehicle- (mock) or DAPT-treated vGPCR- and vFLIP-transduced LEC spheroids.

(E) Sprouting of LECs expressing LANA or v-cyclin and their individual control vectors (mock).

(F) Sprouting of K-LEC spheroids four days after silencing of vGPCR and vFLIP using control siRNAs (si-ctrl), specific siRNAs for vGPCR (si-vGPCR) or vFLIP (si-vFLIP) individually, or simultaneously (si-vGPCR+si-vFLIP). Error bars represent the means of experiments with two different siRNA constructs per condition.

(G) Representative confocal images of the expression of αSMA (upper panels, in red) and fibronectin (lower panels, in green) in K-LEC spheroids in (F).

Scale bars represent 200 μm (A and E), and 100 μm (G). In (A) and (G), nuclei were counterstained with Hoechst 33342 (blue). Error bars in all panels represent the mean fold change with respect to the corresponding mock-treated, vector, or control siRNA controls ± SEM; n = 2 (C [vFLIP] and F), n = 3 (C [vGPCR] and D), and n = 2–4 (B). *$p < 0.05$, **$p < 0.01$, ***$p < 0.001$ (B–D and F). See also Figure S4.

microarray (GEM) profiles of K-LEC spheroids to control LEC spheroids 3 days after embedding to fibrin. The 3D K-LEC transcriptome showed significant upregulation of invasion related genes (GSEA analysis, q = 0.106, FWER p value < 0.0001). The genes with significant change in expression ($p < 0.05$) are shown in Figure 5A. These included genes for proteases *PLAU*, *CTSK*, *ADAMTS1*, and *MMP1*, invasion-linked signaling proteins *SPP1*, *PDGFRA*, *CXCL2*, and *CXCR4,* and transcription factors *ETS2*, *FOXF1*, and *FOXF2* implicated in EMT and invasion, a subset of which has been validated by qRT-PCR (Figure 5B).

To assess the biological relevance of our 3D system to KS, we next compared the K-LEC 3D transcriptome to gene expression profiles of KS biopsies and 2D K-LECs (Wang et al., 2004). This analysis revealed a number of genes coregulated in all three-sample groups (Figure S5A). Intriguingly, the genes with similar coregulation in our system (3D) and KS biopsies included genes involved both in EMT/EndMT and invasive processes (Figure S5B).

As the data suggests that the K-LECs had acquired invasive properties upon reprogramming, and matrix metalloproteinases (MMPs) are key enzymes in cancer cell invasion, we inhibited MMPs in LEC and K-LEC spheroids. A broad-spectrum MMP inhibitor GM6001 significantly reduced the sprouting of K-LEC spheroids (Figure 5C), supporting the necessity of MMPs in sprouting. To assess whether soluble or membrane-associated MMPs were required, we examined the effects of tissue inhibitors of metalloproteinases, TIMP1 and TIMP2. TIMP1 inhibits the secreted, soluble MMPs, including MMP1, MMP2, and MMP9, while TIMP2 widely reduces activity of both soluble MMPs and membrane-bound MT-MMPs (Baker et al., 2002). Whereas treatment with TIMP1 had no effect on the K-LEC spheroids, TIMP2 dramatically inhibited sprouting (Figure 5C), suggesting the involvement of MT-MMPs in the sprouting. Accordingly, a strong upregulation of *MMP14* (gene for MT1-MMP), but not *MMP15* (gene for MT2-MMP) or *MMP16* (gene for MT3-MMP), was

observed in 3D K-LECs by qRT-PCR (Figure S5C). Increased MT1-MMP was also detected by IF of the K-LEC spheroids (Figure S5D).

To functionally assess the invasive properties of LEC and K-LEC cells, we performed an MT-MMP-dependent invasion assay through a crosslinked collagen matrix (Rowe and Weiss, 2009). The results indicate that uninfected LECs lack invasive capacity (~0.3 invading cells per field), whereas K-LECs are able to invade collagen (approximately nine invading cells per field, $p < 0.001$; Figure 5D). These results further suggest that KSHV-induced EndMT involves MT1-MMP-dependent invasiveness. Interestingly, intense MT1-MMP signal was detected predominantly in the KSHV-infected cells (LANA positive) within most of the sections of nodular KS biopsies from one HIV-positive and five HIV-negative patients, whereas it was barely detectable in the surrounding stroma (Figure 5E and Figure S5E). Notably, MT1-MMP was also detected in individual, apparently invasive KSHV-infected cells observed within the surrounding stromal tissue (Figure 5E, arrowheads).

Notch Signaling Induces the 3D K-LECs to Undergo EndMT through MT1-MMP

To further define the requirement of MT1-MMP in EndMT, we depleted MT1-MMP from K-LEC and LEC spheroids (Figure 5F). Depletion of MT1-MMP by two different small interfering RNAs (siRNAs) reduced the sprouting by ~2.0- and ~2.2-fold respectively (Figure 5F), indicating that MT1-MMP is required for efficient K-LEC sprouting in 3D fibrin, and may represent the major MMP involved. MT1-MMP depletion had only a minor effect on expression of Notch target genes *HES1* and *HEY1*, but led to an ~3.3-fold decrease in expression of the mesenchymal marker transgelin (Figure 6A) in the K-LEC spheroids. Interestingly, depletion of MT1-MMP also diminished expression of the *PDGFRB* gene (~2.6-fold; Figure 6A), which is a known effector of EMT (Jechlinger et al., 2006) and cell invasion in fibrin (Lehti et al., 2005). In contrast, treatment of K-LECs with DAPT and Dll4-Fc abolished the induction of MT1-MMP both in 2D and 3D (Figure 6B and data not shown) as well as the 3D-specific induction of *PDGFRB* and *TGLN* (see Figure 3F for DAPT and Figure S3E for Dll4-Fc). These results suggest that MT1-MMP acts downstream of Notch, but is required in 3D for the induction of KSHV-induced EndMT.

To assess further the effects expression of MT1-MMP on the LEC phenotype, we retrovirally overexpressed GFP-tagged MT1-MMP in 3D LECs. Expression of MT1-MMP was confirmed by qRT-PCR (Figure 6C; *MMP14*) and GFP expression (Figure S5F). Outgrowth of sprouts with αSMA expression was seen in the MT1-MMP-expressing LEC spheroids, but not in the mock control (Figure S5F; LEC). Importantly, MT1-MMP expression induced a panel of mesenchymal transcripts including *PDGFRB*, which was abolished by GM6001 (Figure 6C). MT1-MMP did not significantly alter the expression of the Notch target genes, confirming that it acts downstream of Notch and is sufficient to induce LEC invasion and EndMT. These results identify the Notch pathway as a previously unrecognized regulator of MT1-MMP in the sprouting and EndMT in 3D LECs.

Contribution of 3D-Induced PDGFR-β on EndMT

To address the potential role of PDGFR-β in the KSHV-EndMT we inhibited its kinase activity with the reported PDGFR-β inhibitor SU16f (Sun et al., 1999). SU16f treatment led to reduced sprouting in the K-LEC spheroids (Figure S6A) and reduced the expression of mesenchymal markers *TAGLN*, *VIM*, and *CDH2* as well as that of *MMP14*, *PDGFRB* and Notch target gene *HEY1* in K-LEC spheroids (Figure S6B). To assess more specifically the contribution of PDGFR-β in the EndMT we silenced its expression by RNA interference. Unexpectedly, efficient depletion of PDGFR-β led to only a moderate, yet significant reduction in spheroid sprouting and mesenchymal marker expression (Figures 6D and 6E). As the related receptor PDGFR-α is also significantly upregulated in the 3D K-LECs, we sought to determine whether the inhibitor would also target PDGFR-α. Consistent with the results reported by Sun et al. (1999), SU16f dramatically decreased PDGFR-α autophosphorylation in a fibroblast cell line (WI38) with prominent expression of PDGFR-α (Figure S6C). To gain further insight into the role of PDGFR-α in the KSHV-EndMT, we silenced its expression alone or in combination with PDGFR-β. However, depletion of PDGFR-α alone did not affect sprouting, and simultaneous silencing with PDGFR-β did not lead to stronger inhibition on sprouting than PDGFR-β silencing alone (Figure S6D), suggesting that PDGFR-β, but not PDGFR-α, contributes to the KSHV-EndMT (Figure 6F).

3D Microenvironment Leads to Changes in Viral Gene Expression of K-LECs

To investigate whether the microenvironment of the 3D culture and KSHV-induced EndMT involved changes in the pattern of viral gene expression, we carried out qRT-PCR analyses for the expression of latent, early and late lytic transcripts in parental 2D and 3D K-LECs at different time points. By comparison of the mean fold changes of expression between 3D and 2D K-LECs, time-dependent increase in the messenger RNA (mRNA) levels of the latent and lytic viral genes was observed in the 3D cultured K-LECs (Figure 7A). Of note, the mRNA levels of these genes were 2.9- to 8.5-fold increased in 3D over 2D even before embedding the spheroids in fibrin (Figure S7A; day 0), suggesting that the microenvironment during spheroid formation in the non-adherent condition already induces substantial differences in the viral gene expression. Accordingly, a clearly higher proportion of cells expressed the early lytic protein ORF59 in the K-LEC spheroids when compared to the parental K-LECs in 2D and increased over time in 3D culture (Figure 7B). Intriguingly, and in accordance with the increase in LANA mRNA levels in the 3D K-LECs, the majority of the infected cells in K-LEC spheroids (90%) displayed a significantly higher number of nuclear punctate LANA signal by IF (more than ten dots per cell) compared to the parental, infected K-LECs cultured in 2D (about 16%; Figure 7C and Figure S7B). In addition, a time-dependent increase in the viral DNA levels in 3D K-LECs over 2D cells was observed in a real time qPCR analysis on genomic DNA extracted from matching same-day cultures of the cells (Figure S7C).

In a good agreement with their role in KSHV-induced EndMT, both vFLIP and vGPCR transcript levels are elevated in the 3D K-LECs. As Notch has been shown to regulate viral lytic infection via functional interaction with CSL (Liang and Ganem, 2003) we compared expression of a panel of lytic transcripts and the latent LANA mRNA in 3D K-LECs in the presence and absence of DAPT. Although DAPT treatment led to a decrease in the expression of ORF50 and some late lytic genes (vIRF-2, ORF25, and

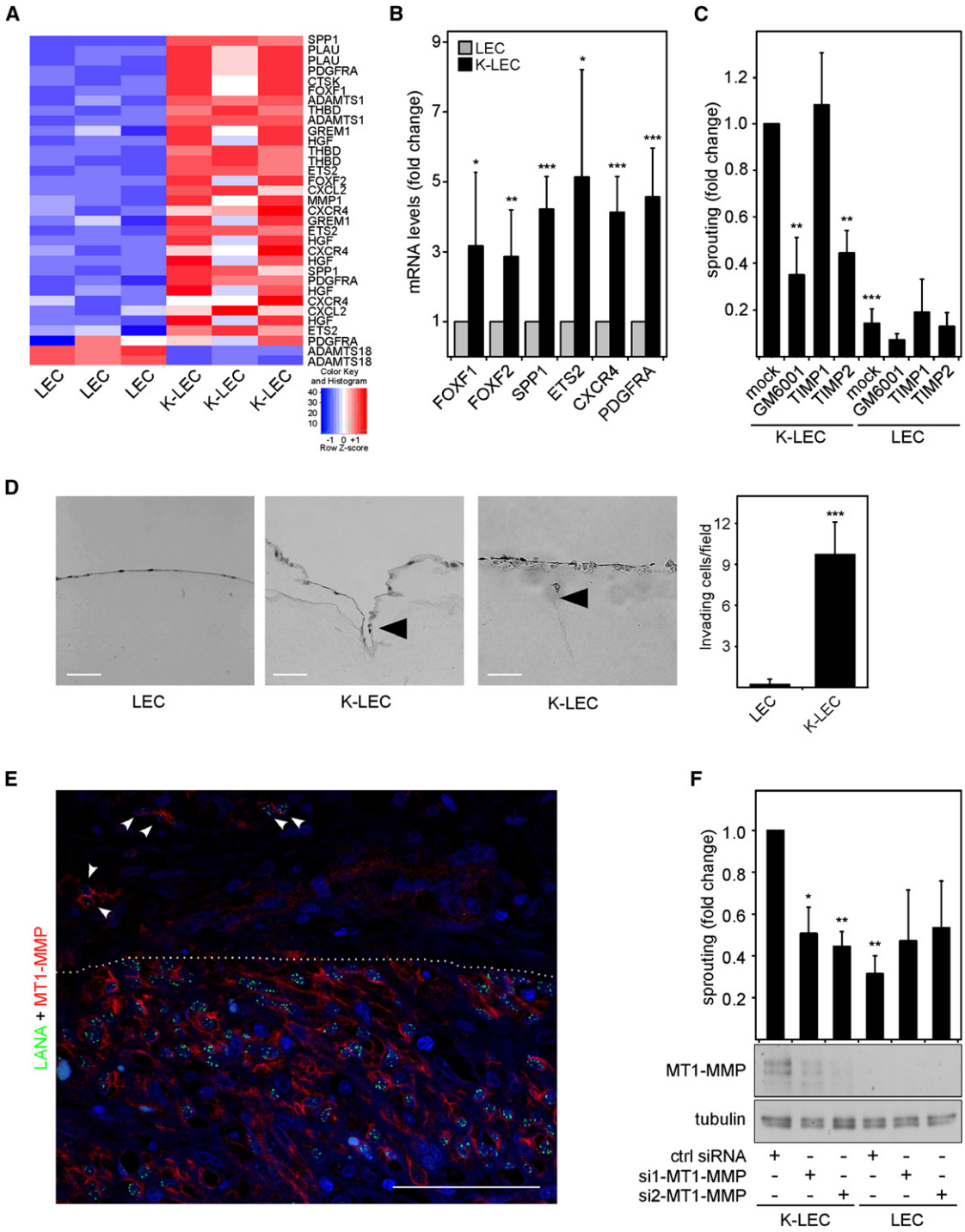

Figure 5. KSHV Endows Primary LECs with MT1-MMP-Dependent Invasive Properties

(A) Heat map representing the most significant relative changes in gene expression of invasion-related genes in 3D LECs after KSHV infection (all probe sets shown, $p < 0.05$). Red and blue denote high and low expression, respectively.

(B) qRT-PCR analysis of mRNA levels for the indicated transcripts in the LEC and K-LEC spheroids.

(C) Inhibition of sprouting of K-LEC and LEC spheroids treated with inhibitors for MMPs (GM6001, TIMP1, and TIMP2) and the respective vehicle controls (mock).

(D) Invasion of control LECs and K-LECs into a 3D collagen matrix. H&E staining of the collagen matrix (left panels; scale bars represent 50 μm) and quantification of the collagen-invading cells (right panel). Arrowhead indicates an invading cell.

(E) Colocalization of LANA (green) and MT1-MMP (red) in a nodular KS biopsy from a HIV-negative patient. Nuclei were counterstained with Hoechst 33342 (blue). The scale bar represents 50 μm. Dashed line denotes the edge of the tumor tissue, and the arrowheads indicate cells invading into the surrounding normal tissue.

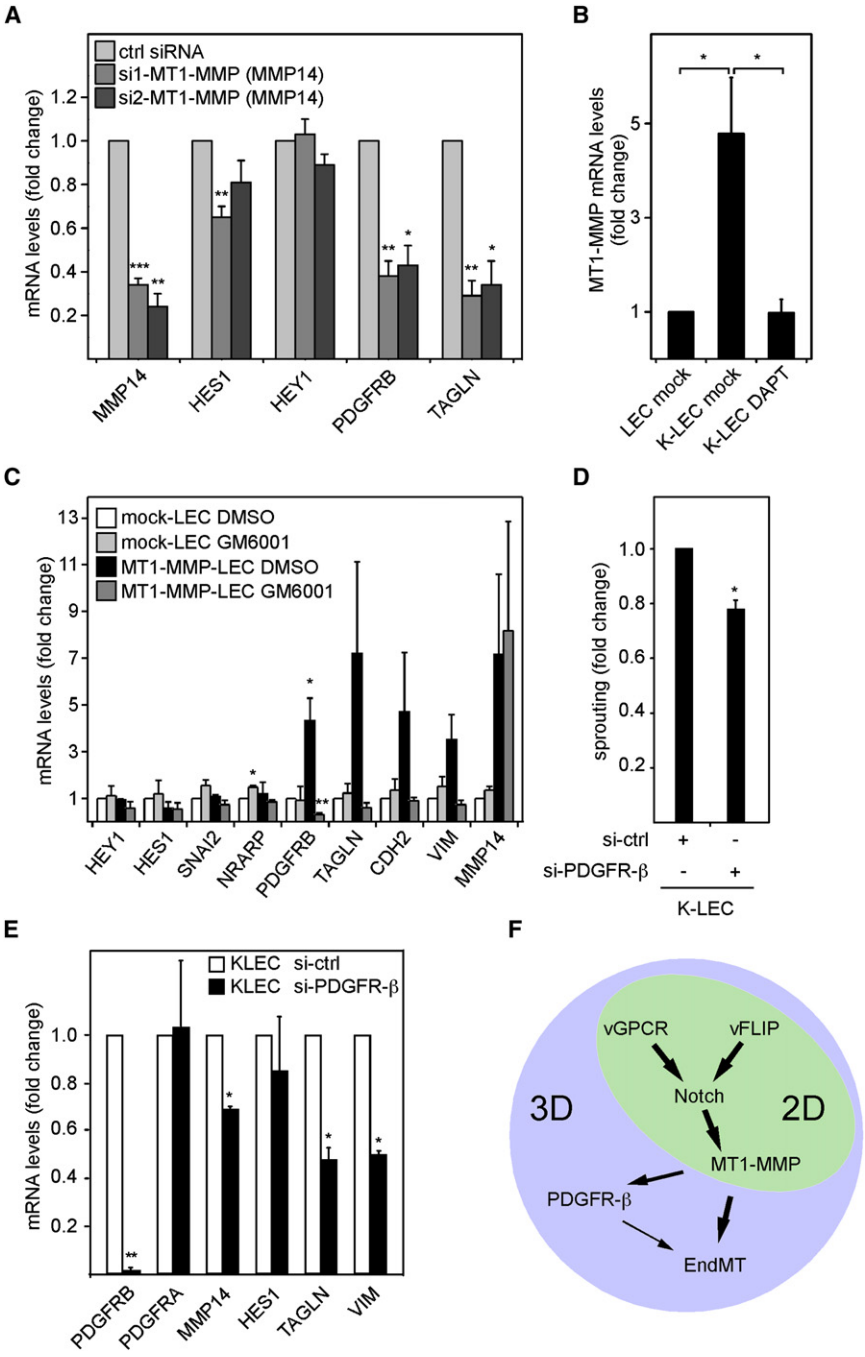

Figure 6. Interplay of Notch, MT1-MMP, and PDGFR-β in the KSHV-Induced EndMT

(A) qRT-PCR analysis for the expression of indicated genes in K-LEC spheroids after depletion of MT1-MMP with specific siRNA oligos (si1-MT1-MMP and si2-MT1-MMP) or control siRNA.

(B) qRT-PCR analysis of mRNA levels of MT1-MMP in K-LEC vehicle- (K-LEC mock) or DAPT-treated (K-LEC DAPT) spheroids.

(C) qRT-PCR analysis for Notch target genes and indicated mesenchymal genes in spheroids of MT1-MMP expressing LECs (MT1-MMP-LEC) or mock-LECs in the presence of GM6001 or the vehicle (DMSO).

(D) Sprouting of the K-LEC spheroids four days after silencing PDGFR-β with specific siRNA oligos (si PDGFR-β) or control siRNA.

(E) qRT-PCR analysis for indicated genes in the K-LEC spheroids after depletion of PDGFR-β as described in D.

(F) Schematic model for the interplay between the Notch, MT1-MMP, and PDGFR-β in the KSHV-induced reprogramming and EndMT.

Error bars in all panels represent the mean fold change with respect to the corresponding mock-treated (B and C), vector, or control siRNA controls (A, D, and E). ± SEM is shown; n = 2 (A–C and E) and n = 3 (D). *p < 0.05, **p < 0.01, ***p < 0.001 (A–E). See also Figure S6.

K8.1), it did not significantly affect expression of LANA, vGPCR or vIL-6 (Figure S7D). To assess the possibility that the late lytic genes would be involved in inducing EndMT, we inhibited their expression, using a well-known inhibitor of lytic replication ganciclovir (GCV) (Kedes and Ganem, 1997). However, this had no effect on sprouting (data not shown) or induction of the Notch target *SNAI2* and mesenchymal transcripts (*MMP14*, *TGLN*, and *VIM*) (Figure S7E).

To address whether the observed gene expression changes involved alterations in the epigenetic landscape of the viral genome, we analyzed histone modification patterns of viral episomes in cells grown under 2D or 3D conditions. We focused on the distribution of H3 molecules that are trimethylated at lysine 4 (H3K4-me3), a modification that is commonly associated with open or active chromatin. ChIP-on-chip analysis revealed no fundamental differences in the overall distribution profile of this histone modification of the viral chromatin between the K-LECs cultured under 3D or 2D conditions at day three (Figure 7D). Both cultures display several prominent peaks that map to the terminal repeat regions, the genomic segment spanning open reading frames (ORFs) K2 to K7, as well as to regions that encode Kaposin, the viral microRNAs, ORF72, ORF71 and the latency promoter-proximal region of ORF73 (Figure 7D). It should

(F) Top: Inhibition of sprouting of K-LEC and LEC spheroids by silencing MT1-MMP with specific siRNA oligos (si1-MT1-MMP and si2-MT1-MMP). Bottom: Western blot analysis with anti-MT1-MMP antibodies.

Error bars in all panels represent mean fold change with respect to the corresponding control (LEC in B and D; mock in C, and ctrl siRNA in F). In (B), ± SD is shown, n = 4–5; in (C), ± SD is shown, n = 2–4; in (D), ± SD is shown, n = 2, and in (F), ± SEM is shown, n = 2–3. *p < 0.05, **p < 0.01, ***p < 0.001 (B–D and F). See also Figure S5.

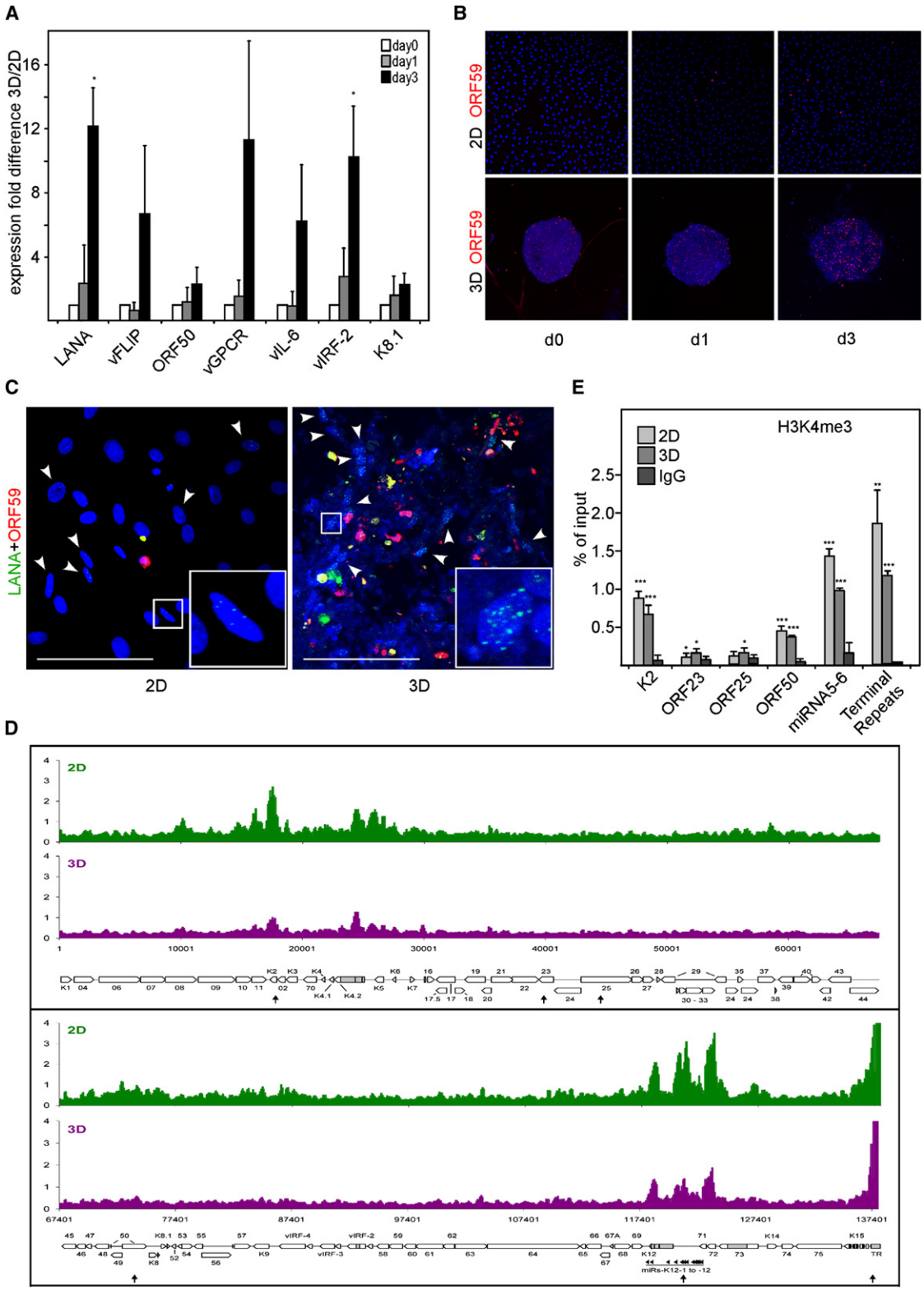

Figure 7. 3D Microenvironment Induces Changes in the Viral Gene Expression of K-LECs

(A) qRT-PCR analysis for the expression of latent KSHV genes *LANA* and *vFLIP* and lytic genes *ORF50*, *vGPCR*, *vIL-6*, *vIRF-2*, and *K8.1* at three different time points (day 0, 1, and 3). Error bars represent a mean fold change of expression in K-LEC 3D over 2D. The value for each gene in the 2D and 3D time points was normalized to the corresponding day 0 values in 2D or 3D, respectively. ± SEM is shown; n = 3–5.

(B) Expression of the lytic protein ORF59 in the parental 2D (K-LEC 2D) and 3D K-LECs (K-LEC 3D) at three different time points (day 0, 1, and 3).

be pointed out though that the peaks appear to be less prominent in the 3D cultures (Figure 7D), a result that was also confirmed by qRT-PCR (Figure 7E). However, since the principal peak distribution of H4K4-m3 marks appears unaffected, we conclude that global changes of H3K4-me3 marks are unlikely to be responsible for the viral gene expression changes observed between the 3D and 2D cultures. An interesting possibility is that such changes may instead result from the loss of repressive marks such as H3K27-me3. This histone modification has previously been found to be present on latent KSHV episomes, where it suppresses lytic gene expression via recruitment of polycomb repressor complexes (Günther and Grundhoff, 2010; Toth et al., 2010). A loss of H3K27-me3 would be expected to result in increased gene expression from loci that are otherwise in a transcription-competent state, e.g., those which carry activation marks such as H3K4-me3.

DISCUSSION

Here, we demonstrate that KSHV reprograms primary LECs to mesenchymal cells via EndMT, suggesting that the heterogeneity of cell types in KS lesions could originate from the infected endothelium via this process. The data further identifies Notch as a previously unrecognized upstream regulator of MT1-MMP, and demonstrates that MT1-MMP is sufficient to provide LECs with a mechanism to undergo EndMT in 3D. We also show induction of PDGFR-β by the Notch MT1-MMP axis in the EndMT, which concurs with an earlier report linking Notch 4-mediated upregulation of PDGFR to EndMT (Noseda et al., 2004). Moreover, culturing K-LECs in the 3D microenvironment led to intriguing changes in the pattern of viral gene expression.

The Notch pathway has been implicated in both KSHV latency (Lan et al., 2007) and lytic replication (Chang et al., 2005). Accordingly, Notch 1–Notch 4 are reported to be expressed in KS tumors (Curry et al., 2005). Consistent with previous reports (Emuss et al., 2009; Liu et al., 2010), the KSHV-induced reprogramming was initiated by the engagement of Notch pathway already in 2D. However, the transition into mesenchymal phenotype required both a microenvironment provided here by the crosslinked 3D fibrin matrix, and intact microtubule dynamics to support the ingression into the 3D matrix. Contrary to our data, induction of mural cell markers was recently reported in 2D cultured HPV-16 E6/E7-immortalized LECs stably infected by rKSHV (Liu et al., 2010). This could be due to the sensitizing effect of ectopic E6 and E7, as overexpression of these genes has previously been implicated in EMT induction (Hellner et al., 2009).

The consequence of Notch inhibition in our 3D system, i.e., the significant attenuation of K-LEC sprouting and EndMT differs significantly from the effect of Notch inhibition on blood ECs and angiogenesis (Ridgway et al., 2006; Zheng et al., 2011). Moreover, stimulation of K-LECs by VEGF-A/C induced a dramatic outgrowth of capillary sprouts in 3D, and a simultaneous inhibition of EndMT. This suggests that the mesenchymal sprouting of K-LECs represents a distinct biological process that dominates over the (lymph)angiogenic sprouting in the absence of VEGF-A/C stimulation. These results further corroborate the central role of Notch signaling in cell-fate determination, and as a critical determinant for the lymphangiogenic versus mesenchymal fate of LECs.

Our results reveal a 3D environment dependent function of MT1-MMP as an EndMT inducer in LECs, which is consistent with the ability of MT1-MMP to induce an invasive EMT program in MCF7 cells in 3D environment, although the cells retain their epithelial morphology in 2D culture. Although the mechanisms by which MT1-MMP mediates such effects remain to be established, it is important to bear in mind that MT1-MMP has hundreds of potential extracellular matrix (ECM) and non-ECM substrates (Butler et al., 2008). In the case of EMT or EndMT, MT1-MMP-mediated proteolysis could also indirectly affect gene expression by altering local ECM rigidity, cell shape, and tension (Rowe and Weiss, 2009). Along these lines, MT1-MMP also interacts with membrane receptors including integrins, FGFRs, and PDGFRs, thus altering the receptor functions and cell phenotype (Lehti et al., 2005; Sugiyama et al., 2010). In the context of K-LECs, where KSHV-induced Notch activation first upregulated MT1-MMP already in 2D KLECs, both MT1-MMP itself and PDGFR-β were part of the transcriptional EndMT program induced by Notch/MT1-MMP axis in 3D environment. As a potent regulator of mesenchymal cell invasion, proliferation, and differentiation, PDGFR-β cooperated as a logical partner with MT1-MMP in EndMT.

Primary LECs normally express very low levels of MT-MMPs (Petrova et al., 2002). Here, we demonstrate that KSHV reprogramming induces a substantial MT1-MMP upregulation in the KSHV-infected LECs, resulting in cell invasive activities in 3D fibrin and collagen. This is in striking contrast to MT1-MMP expression during angiogenesis where it is confined largely to the tip cell of the sprouting neovessels (Yana et al., 2007). In several human cancers MT1-MMP serves as a critical regulator of both growth and dissemination of tumor cells (Rowe and Weiss, 2009). We further identify MT1-MMP as a prominent marker of KSHV-infected cells in KS tumors. MT1-MMP was also expressed in the single LANA-positive, KSHV-infected cells in the surrounding stromal tissue. They can represent infected cells that mediate spreading and persistence of the infection via invasion and dissemination from the primary site. In support of this proposal, the K-LEC spheroids showed a time-dependent increase in the number of the nuclear punctate LANA dots per cell and amount of viral DNA over the parental 2D cultures,

(C) Expression of LANA (green) in the parental 2D (2D) and 3D K-LEC (3D) cultures at day 3. Cells were double stained for the expression of the lytic protein ORF59 (red). Insets show a magnification of the cell indicated with a white box. Arrowheads point to LANA-positive cells in the images.
(D and E) Global patterns of H3K4 tri-methylation (H3K4-me3) in parental 2D and 3D K-LEC cultures (D; upper and lower plots, respectively, in each panel). Values shown on the y axis represent enrichment of normalized signals obtained with an H3K4-me3 specific antibody relative to IgG isotype control. Nucleotide positions and genome map shown at the bottom of each panel refer to the reference KSHV sequence (NC_009333). ORFs and repeat regions are indicated as block arrows and gray boxes, respectively. Arrows in (D) indicate six genomic loci for which qRT-PCR analysis was done in (E) to confirm the array data as the observed enrichment of immunoprecipitated versus input levels for H3K27-me3 or negative control IgG. ± SEM is shown; n=2.
In (B) and (C), nuclei were counterstained with Hoechst 33342 (blue). Scale bars represent 100 μm. *$p < 0.05$, **$p < 0.01$, ***$p < 0.001$ (A and E). See also Figure S7.

suggesting that the 3D environment could be more permissive for viral replication. The number of individual LANA dots per cell has been shown to be predictive of intracellular viral genome load (Adang et al., 2006). Therefore the apparently higher viral load in the 3D K-LECs could be due to increased latent replication, improved maintenance of viral episomes or re-infection of the cells as a result of activated lytic program upon change from 2D to 3D microenvironment.

Taken together, our results suggest that Notch signaling is activated in K-LECs by the KSHV proteins vGPCR and vFLIP, which in turn leads to Notch-dependent induction of MT1-MMP. Consistently, exogenous vGPCR expression has previously been linked to MT1-MMP upregulation in pulmonary arterial endothelial cells (Shan et al., 2007). The activated Notch and MT1-MMP were not sufficient for the virus-induced EndMT in 2D, which required the crosslinked 3D fibrin matrix. Signals provided by the 3D microenvironment led to a further increase in MT1-MMP and induction of mesenchymal markers (see Figure 6F for a schematic model). In light of these findings, we propose that the KSHV-induced invasive mesenchymal cell phenotype could contribute to the development of KS, and help to explain the progression of the disease through spread of the infected cells into surrounding connective tissue.

EXPERIMENTAL PROCEDURES

Cell Lines and Cell Culture

The BCBL-1 cells were provided by A. Moses (Oregon Health and Science University) or through the National Institutes of Health AIDS Research and Reference Reagent Program (catalog number 3233 from McGrath and Ganem), and cultured in RPMI 1640 medium supplemented with 10% fetal calf serum (FCS; Invitrogen), 100 U/ml penicillin, and 100 μg/ml streptomycin. Primary juvenile foreskin lymphatic endothelial cells (LECs; PromoCell) were cultured in the basal EC medium plus supplements (PromoCell), in the presence of 5% human serum, 25 μg/ml amphotericin B, and 25 μg/ml gentamycin. rKSHV-Vero cells (Vieira and O'Hearn, 2004) (a kind gift of J. Vieira, University of Washington), U2OS human osteosarcoma cell line (obtained from the American Type Culture Collection [ATCC]), and WI-38 human embryonic lung fibroblasts (ATCC CCL-75, obtained from ATCC) were cultured in Dulbecco modified Eagle's medium (DMEM) containing 10% FCS, 100 U/ml penicillin, 100 μg/ml streptomycin, and 5 μg/ml puromycin. All cells were cultured in a humidified 5% CO_2 atmosphere at 37°C.

KSHV Infection of LECs

For infection, the LECs were split at a density of 2.5 × 10^5 cells per a 6-well, and spin-infected with multiplicity of infection (MOI) of ~3 in serum-free medium with 8 μg/ml polybrene. In the K-LEC cultures, the WT KSHV infection efficiency was 20%–40% by LANA staining or 30%–50% with recombinant rKSHV.219 by GFP expression. To produce inactivated virus (UV-KSHV), an aliquot of freshly produced KSHV was treated by 3000 mJ of UV-C light with UV Stratalinker 1800 (Stratagene), and the loss of infectivity was confirmed by measurement of the virus titer.

Generation of LEC Spheroids

Confluent monolayers of spindling K-LECs or uninfected control LECs were seeded into 0.5% agarose precoated, nonadherent round-bottom 96-well plates at 4000 cells per well. After 16 hr to 24 hr incubation at 37°C, the formed spheroids were harvested and embedded into the fibrin gel consisting of plasminogen-free human fibrinogen (final concentration 3 mg/ml; Calbiochem) and human thrombin (final concentration 2 U/ml; Sigma) in 50 μl Hank's Balanced Salt Solution supplemented with 400 μg/ml aprotinin (Sigma). The gels were cast onto the bottom of 24-well plates and incubated for 1 hr at 37°C to allow complete gelling followed by addition of EC culture medium and followed for 2–5 days.

Quantification of Spheroid Sprouting

Quantification of spheroid sprouting was performed from the phase contrast images with the Inkscape software (http://www.inkscape.org/), and then analyzed in a pipeline created in the Anduril framework (Ovaska et al., 2010). For a detailed description of this, see the Supplemental Experimental Procedures.

Chemicals and Treatments

The inhibitors and ligands used are described in the Supplemental Experimental Procedures. Human VEGF-A and VEGF-C were included in the medium 1 day before spheroid preparation, during spheroid formation, and for 2 days in 3D. WI-38 cells were treated with PDGF-AA and PDGF-BB for 10 min after SU16f treatment for 24 hr to address the phosho-Tyrosine (pTyr) signal by immunoprecipitation and immunoblotting. Unless stated otherwise, the inhibitors were added into the medium after the spheroids were embedded into the fibrin gel and followed for 2–4 days.

Invasion Assay

Collagen invasion was assessed essentially as described (Hotary et al., 2000). For a detailed description of this, see the Supplemental Experimental Procedures.

Statistical Analysis

For statistical evaluation of qRT-PCR data, the values (logarithmic) were converted to ddCt values (linear log2 scale values) and p values were calculated with a one-tailed unpaired Student's t test. The p values for sprouting and inhibition of gene expression were calculated directly from the data normalized to the appropriate control.

Accession numbers

Microarray data are deposited in NCBI GEO under accession number GSE22522 (http://www.ncbi.nlm.nih.gov/geo/query/acc.cgi?token=vxqvzoiuuqwaenw&acc=GSE22522).

SUPPLEMENTAL INFORMATION

Supplemental Information includes Supplemental Experimental Procedures, seven figures, and one table and can be found with this article online at doi:10.1016/j.chom.2011.10.011.

ACKNOWLEDGMENTS

We thank T. Tammela, W. Zheng, B. Chandran, K. Koli, J. Keski-Oja, T. Mäkelä, A. Vaheri, A. Moses, J. Vieira, P. Laakkonen, and the National Institutes of Health AIDS Research and Reference Reagent Program for reagents and cell lines. R. Ruhl is thanked for advice on virus production, and D. Kedes is thanked for advice on virus titering. J. Bärlund, A. Aarnio, L. Ma, S. Nieminen, and I. Vuoristo are acknowledged for excellent technical assistance, and the Biomedicum Genomics and Biomedicum Imaging Unit is acknowledged for providing expert service on GEM and imaging. This work was supported by grants from the Academy of Finland (P.M.O. and K.L.), University of Helsinki Foundations (P.M.O. and K.L.), Finnish Cancer Foundations (P.M.O.), Sigrid Juselius Foundation (P.M.O.), and European Union (FP6 INCA project LSHC-CT-2005-018704) to P.M.O. S.L. was supported by the Finnish Cultural Foundation and Paulo Foundation, F.C., P.P., and E.K. by the Helsinki Biomedical Graduate School, and N.S. by the Finnish Graduate School of Musculoskeletal Disorders and Biomaterials.

Received: February 18, 2011
Revised: June 6, 2011
Accepted: October 31, 2011
Published: December 14, 2011

REFERENCES

Adang, L.A., Parsons, C.H., and Kedes, D.H. (2006). Asynchronous progression through the lytic cascade and variations in intracellular viral loads revealed

by high-throughput single-cell analysis of Kaposi's sarcoma-associated herpesvirus infection. J. Virol. *80*, 10073–10082.

Baker, A.H., Edwards, D.R., and Murphy, G. (2002). Metalloproteinase inhibitors: biological actions and therapeutic opportunities. J. Cell Sci. *115*, 3719–3727.

Butler, G.S., Dean, R.A., Tam, E.M., and Overall, C.M. (2008). Pharmacoproteomics of a metalloproteinase hydroxamate inhibitor in breast cancer cells: dynamics of membrane type 1 matrix metalloproteinase-mediated membrane protein shedding. Mol. Cell. Biol. *28*, 4896–4914.

Carroll, P.A., Brazeau, E., and Lagunoff, M. (2004). Kaposi's sarcoma-associated herpesvirus infection of blood endothelial cells induces lymphatic differentiation. Virology *328*, 7–18.

Chang, H., Dittmer, D.P., Shin, Y.C., Hong, Y., and Jung, J.U. (2005). Role of Notch signal transduction in Kaposi's sarcoma-associated herpesvirus gene expression. J. Virol. *79*, 14371–14382.

Curry, C.L., Reed, L.L., Golde, T.E., Miele, L., Nickoloff, B.J., and Foreman, K.E. (2005). Gamma secretase inhibitor blocks Notch activation and induces apoptosis in Kaposi's sarcoma tumor cells. Oncogene *24*, 6333–6344.

Dupin, N., Fisher, C., Kellam, P., Ariad, S., Tulliez, M., Franck, N., van Marck, E., Salmon, D., Gorin, I., Escande, J.P., et al. (1999). Distribution of human herpesvirus-8 latently infected cells in Kaposi's sarcoma, multicentric Castleman's disease, and primary effusion lymphoma. Proc. Natl. Acad. Sci. USA *96*, 4546–4551.

Emuss, V., Lagos, D., Pizzey, A., Gratrix, F., Henderson, S.R., and Boshoff, C. (2009). KSHV manipulates Notch signaling by DLL4 and JAG1 to alter cell cycle genes in lymphatic endothelia. PLoS Pathog. *5*, e1000616.

Ganem, D. (2010). KSHV and the pathogenesis of Kaposi sarcoma: listening to human biology and medicine. J. Clin. Invest. *120*, 939–949.

Grundhoff, A., and Ganem, D. (2004). Inefficient establishment of KSHV latency suggests an additional role for continued lytic replication in Kaposi sarcoma pathogenesis. J. Clin. Invest. *113*, 124–136.

Günther, T., and Grundhoff, A. (2010). The epigenetic landscape of latent Kaposi sarcoma-associated herpesvirus genomes. PLoS Pathog. *6*, e1000935.

Hellner, K., Mar, J., Fang, F., Quackenbush, J., and Münger, K. (2009). HPV16 E7 oncogene expression in normal human epithelial cells causes molecular changes indicative of an epithelial to mesenchymal transition. Virology *391*, 57–63.

Hong, Y.K., Foreman, K., Shin, J.W., Hirakawa, S., Curry, C.L., Sage, D.R., Libermann, T., Dezube, B.J., Fingeroth, J.D., and Detmar, M. (2004). Lymphatic reprogramming of blood vascular endothelium by Kaposi sarcoma-associated herpesvirus. Nat. Genet. *36*, 683–685.

Hotary, K., Allen, E., Punturieri, A., Yana, I., and Weiss, S.J. (2000). Regulation of cell invasion and morphogenesis in a three-dimensional type I collagen matrix by membrane-type matrix metalloproteinases 1, 2, and 3. J. Cell Biol. *149*, 1309–1323.

Jechlinger, M., Sommer, A., Moriggl, R., Seither, P., Kraut, N., Capodiecci, P., Donovan, M., Cordon-Cardo, C., Beug, H., and Grünert, S. (2006). Autocrine PDGFR signaling promotes mammary cancer metastasis. J. Clin. Invest. *116*, 1561–1570.

Kaaya, E.E., Parravicini, C., Ordonez, C., Gendelman, R., Berti, E., Gallo, R.C., and Biberfeld, P. (1995). Heterogeneity of spindle cells in Kaposi's sarcoma: comparison of cells in lesions and in culture. J. Acquir. Immune Defic. Syndr. Hum. Retrovirol. *10*, 295–305.

Kalluri, R., and Weinberg, R.A. (2009). The basics of epithelial-mesenchymal transition. J. Clin. Invest. *119*, 1420–1428.

Kedes, D.H., and Ganem, D. (1997). Sensitivity of Kaposi's sarcoma-associated herpesvirus replication to antiviral drugs. Implications for potential therapy. J. Clin. Invest. *99*, 2082–2086.

Koopal, S., Furuhjelm, J.H., Järviluoma, A., Jäämaa, S., Pyakurel, P., Pussinen, C., Wirzenius, M., Biberfeld, P., Alitalo, K., Laiho, M., and Ojala, P.M. (2007). Viral oncogene-induced DNA damage response is activated in Kaposi sarcoma tumorigenesis. PLoS Pathog. *3*, 1348–1360.

Korff, T., and Augustin, H.G. (1998). Integration of endothelial cells in multicellular spheroids prevents apoptosis and induces differentiation. J. Cell Biol. *143*, 1341–1352.

Lagunoff, M., Bechtel, J., Venetsanakos, E., Roy, A.M., Abbey, N., Herndier, B., McMahon, M., and Ganem, D. (2002). De novo infection and serial transmission of Kaposi's sarcoma-associated herpesvirus in cultured endothelial cells. J. Virol. *76*, 2440–2448.

Lan, K., Verma, S.C., Murakami, M., Bajaj, B., Kaul, R., and Robertson, E.S. (2007). Kaposi's sarcoma herpesvirus-encoded latency-associated nuclear antigen stabilizes intracellular activated Notch by targeting the Sel10 protein. Proc. Natl. Acad. Sci. USA *104*, 16287–16292.

Lehti, K., Allen, E., Birkedal-Hansen, H., Holmbeck, K., Miyake, Y., Chun, T.H., and Weiss, S.J. (2005). An MT1-MMP-PDGF receptor-beta axis regulates mural cell investment of the microvasculature. Genes Dev. *19*, 979–991.

Liang, Y., and Ganem, D. (2003). Lytic but not latent infection by Kaposi's sarcoma-associated herpesvirus requires host CSL protein, the mediator of Notch signaling. Proc. Natl. Acad. Sci. USA *100*, 8490–8495.

Liu, R., Li, X., Tulpule, A., Zhou, Y., Scehnet, J.S., Zhang, S., Lee, J.S., Chaudhary, P.M., Jung, J., and Gill, P.S. (2010). KSHV-induced notch components render endothelial and mural cell characteristics and cell survival. Blood *115*, 887–895.

Mansouri, M., Douglas, J., Rose, P.P., Gouveia, K., Thomas, G., Means, R.E., Moses, A.V., and Früh, K. (2006). Kaposi sarcoma herpesvirus K5 removes CD31/PECAM from endothelial cells. Blood *108*, 1932–1940.

McAllister, S.C., and Moses, A.V. (2007). Endothelial cell- and lymphocyte-based in vitro systems for understanding KSHV biology. Curr. Top. Microbiol. Immunol. *312*, 211–244.

Medici, D., Shore, E.M., Lounev, V.Y., Kaplan, F.S., Kalluri, R., and Olsen, B.R. (2010). Conversion of vascular endothelial cells into multipotent stem-like cells. Nat. Med. *16*, 1400–1406.

Mutlu, A.D., Cavallin, L.E., Vincent, L., Chiozzini, C., Eroles, P., Duran, E.M., Asgari, Z., Hooper, A.T., La Perle, K.M., Hilsher, C., et al. (2007). In vivo-restricted and reversible malignancy induced by human herpesvirus-8 KSHV: a cell and animal model of virally induced Kaposi's sarcoma. Cancer Cell *11*, 245–258.

Noseda, M., McLean, G., Niessen, K., Chang, L., Pollet, I., Montpetit, R., Shahidi, R., Dorovini-Zis, K., Li, L., Beckstead, B., et al. (2004). Notch activation results in phenotypic and functional changes consistent with endothelial-to-mesenchymal transformation. Circ. Res. *94*, 910–917.

Ovaska, K., Laakso, M., Haapa-Paananen, S., Louhimo, R., Chen, P., Aittomäki, V., Valo, E., Núñez-Fontarnau, J., Rantanen, V., Karinen, S., et al. (2010). Large-scale data integration framework provides a comprehensive view on glioblastoma multiforme. Genome Med *2*, 65.

Petrova, T.V., Mäkinen, T., Mäkelä, T.P., Saarela, J., Virtanen, I., Ferrell, R.E., Finegold, D.N., Kerjaschki, D., Ylä-Herttuala, S., and Alitalo, K. (2002). Lymphatic endothelial reprogramming of vascular endothelial cells by the Prox-1 homeobox transcription factor. EMBO J. *21*, 4593–4599.

Potenta, S., Zeisberg, E., and Kalluri, R. (2008). The role of endothelial-to-mesenchymal transition in cancer progression. Br. J. Cancer *99*, 1375–1379.

Qian, L.W., Greene, W., Ye, F., and Gao, S.J. (2008). Kaposi's sarcoma-associated herpesvirus disrupts adherens junctions and increases endothelial permeability by inducing degradation of VE-cadherin. J. Virol. *82*, 11902–11912.

Ridgway, J., Zhang, G., Wu, Y., Stawicki, S., Liang, W.C., Chanthery, Y., Kowalski, J., Watts, R.J., Callahan, C., Kasman, I., et al. (2006). Inhibition of Dll4 signalling inhibits tumour growth by deregulating angiogenesis. Nature *444*, 1083–1087.

Rowe, R.G., and Weiss, S.J. (2009). Navigating ECM barriers at the invasive front: the cancer cell-stroma interface. Annu. Rev. Cell Dev. Biol. *25*, 567–595.

Shan, B., Morris, C.A., Zhuo, Y., Shelby, B.D., Levy, D.R., and Lasky, J.A. (2007). Activation of proMMP-2 and Src by HHV8 vGPCR in human pulmonary arterial endothelial cells. J. Mol. Cell. Cardiol. *42*, 517–525.

Stürzl, M., Brandstetter, H., Zietz, C., Eisenburg, B., Raivich, G., Gearing, D.P., Brockmeyer, N.H., and Hofschneider, P.H. (1995). Identification of interleukin-1

and platelet-derived growth factor-B as major mitogens for the spindle cells of Kaposi's sarcoma: a combined in vitro and in vivo analysis. Oncogene *10*, 2007–2016.

Sugiyama, N., Varjosalo, M., Meller, P., Lohi, J., Chan, K.M., Zhou, Z., Alitalo, K., Taipale, J., Keski-Oja, J., and Lehti, K. (2010). FGF receptor-4 (FGFR4) polymorphism acts as an activity switch of a membrane type 1 matrix metalloproteinase-FGFR4 complex. Proc. Natl. Acad. Sci. USA *107*, 15786–15791.

Sun, L., Tran, N., Liang, C., Tang, F., Rice, A., Schreck, R., Waltz, K., Shawver, L.K., McMahon, G., and Tang, C. (1999). Design, synthesis, and evaluations of substituted 3-[(3- or 4-carboxyethylpyrrol-2-yl)methylidenyl]indolin-2-ones as inhibitors of VEGF, FGF, and PDGF receptor tyrosine kinases. J. Med. Chem. *42*, 5120–5130.

Timmerman, L.A., Grego-Bessa, J., Raya, A., Bertrán, E., Pérez-Pomares, J.M., Díez, J., Aranda, S., Palomo, S., McCormick, F., Izpisúa-Belmonte, J.C., and de la Pompa, J.L. (2004). Notch promotes epithelial-mesenchymal transition during cardiac development and oncogenic transformation. Genes Dev. *18*, 99–115.

Toth, Z., Maglinte, D.T., Lee, S.H., Lee, H.R., Wong, L.Y., Brulois, K.F., Lee, S., Buckley, J.D., Laird, P.W., Marquez, V.E., and Jung, J.U. (2010). Epigenetic analysis of KSHV latent and lytic genomes. PLoS Pathog. *6*, e1001013.

Vieira, J., and O'Hearn, P.M. (2004). Use of the red fluorescent protein as a marker of Kaposi's sarcoma-associated herpesvirus lytic gene expression. Virology *325*, 225–240.

Wang, H.W., Trotter, M.W., Lagos, D., Bourboulia, D., Henderson, S., Mäkinen, T., Elliman, S., Flanagan, A.M., Alitalo, K., and Boshoff, C. (2004). Kaposi sarcoma herpesvirus-induced cellular reprogramming contributes to the lymphatic endothelial gene expression in Kaposi sarcoma. Nat. Genet. *36*, 687–693.

Weich, H.A., Salahuddin, S.Z., Gill, P., Nakamura, S., Gallo, R.C., and Folkmann, J. (1991). AIDS-associated Kaposi's sarcoma-derived cells in long-term culture express and synthesize smooth muscle alpha-actin. Am. J. Pathol. *139*, 1251–1258.

Yana, I., Sagara, H., Takaki, S., Takatsu, K., Nakamura, K., Nakao, K., Katsuki, M., Taniguchi, S., Aoki, T., Sato, H., et al. (2007). Crosstalk between neovessels and mural cells directs the site-specific expression of MT1-MMP to endothelial tip cells. J. Cell Sci. *120*, 1607–1614.

Zheng, W., Tammela, T., Yamamoto, M., Anisimov, A., Holopainen, T., Kaijalainen, S., Karpanen, T., Lehti, K., Ylä-Herttuala, S., and Alitalo, K. (2011). Notch restricts lymphatic vessel sprouting induced by vascular endothelial growth factor. Blood *118*, 1154–1162.